ADVANCED OPTICAL MATERIALS

Supporting Information

for *Adv. Optical Mater.*, DOI: 10.1002/adom.201600039

Wide-Field Optical Microscopy of Microwave Fields Using Nitrogen-Vacancy Centers in Diamonds

*Linbo Shao, Ruishan Liu, Mian Zhang, Anna V. Shneidman, Xavier Audier, Matthew Markham, Harpreet Dhillon, Daniel J. Twitchen, Yun-Feng Xiao, and Marko Lonc#ar**

Wide-field Optical Microscopy of Microwave Fields Using Nitrogen-Vacancy Centers in Diamonds
Supplementary Information

Linbo Shao,[1] Ruishan Liu,[1,2] Mian Zhang,[1] Anna V. Shneidman,[1,3] Xavier Audier,[1] Matthew Markham,[4] Harpreet Dhillon,[4] Daniel J. Twitchen,[4] Yun-Feng Xiao,[2] and Marko Lončar[1,*]

[1]*School of Engineering and Applied Science, Harvard University, 29 Oxford Street, Cambridge, MA 02138, USA*

[2]*State Key Laboratory for Mesoscopic Physics and School of Physics, Peking University, 5 Yiheyuan Road, Beijing, 100871, China*

[3]*Department of Chemistry and Chemical Biology, Harvard University, 12 Oxford Street, Cambridge, MA 02138, USA*

[4]*Element 6, Element Six Innovation, Fermi Avenue, Harwell Oxford, Didcot, Oxfordshire OX110QR, UK*

Additional information for experiments and theoretical analysis are provided in this *Supplementary Information*.

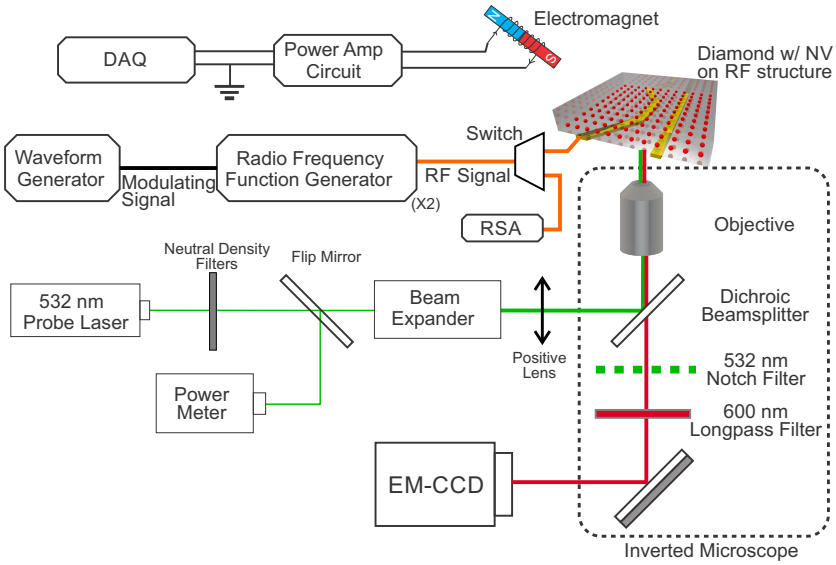

FIG. S1: Detailed experimental setup. The experimental setup is described in *Experimental Section*. DAQ is data acquisition device, RSA is real-time spectrum analyzer, EM-CCD is electron-multiplying charge coupled device.

*Electronic address: loncar@seas.harvard.edu

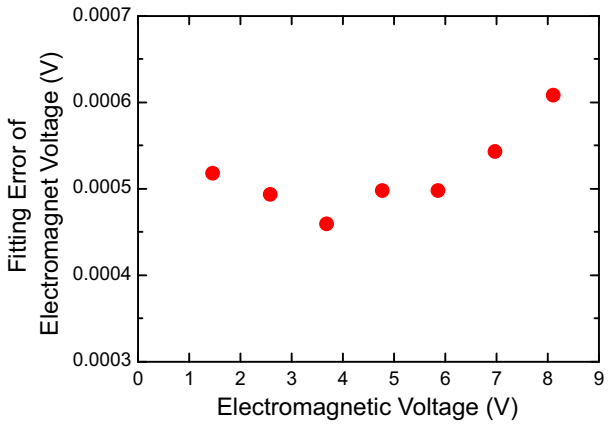

FIG. S2: Errors in fitting of resonant frequencies. Each point depicts the errors of three Lorentz dips fitting corresponding to the point in Fig. 2(b).

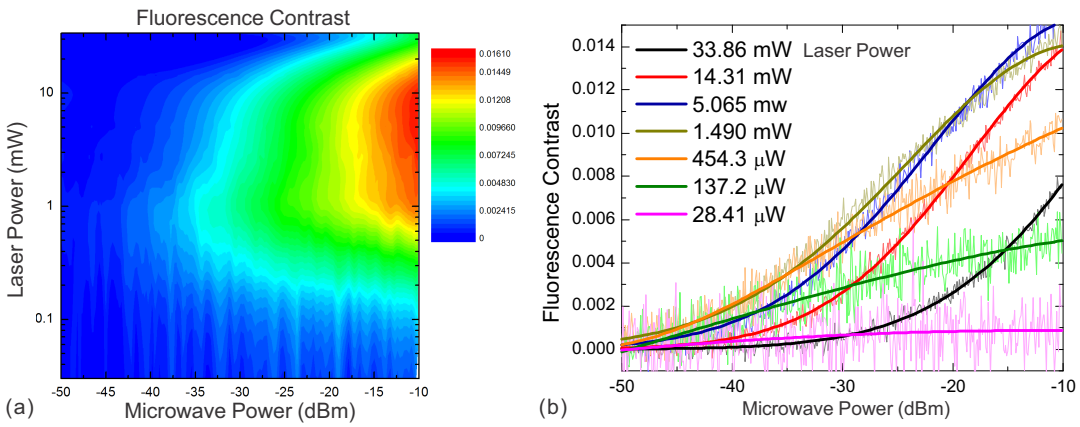

FIG. S3: Dependence of fluorescence contrast on laser power and microwave power. (a) The 2D color mapping of fluorescence contrast as a function of probe laser power and microwave signal power. (b) Fluorescence contrast, showing additional data points than Fig. 2(d).

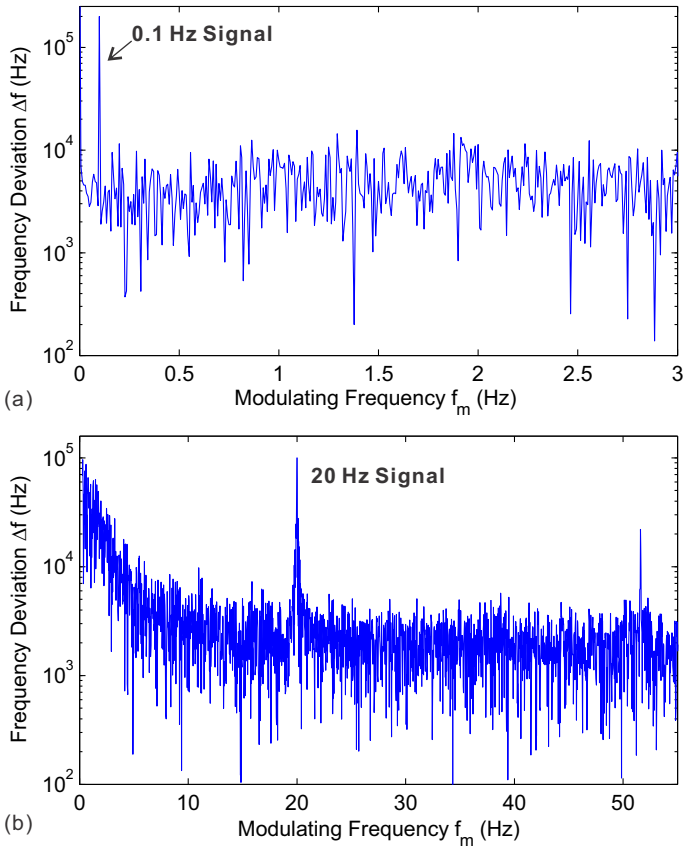

FIG. S4: Signal and noise spectra in FM detection. (a) the spectrum of signal in Fig. 4(b), showing a modulating signal of $f_m = 0.1$ Hz. (b) the spectrum of signal in Fig. 4(g) at higher capture rate, showing a modulating signal of $f_m = 20$ Hz.

Note 1. ESTIMATION OF AMPLITUDE SENSITIVITY

Here we estimate amplitude sensitivity of microwave field in terms of magnetic field amplitude. Consistent with in Fig. 2(d), the sensitivity is estimated for the 5×5 μm^2 region near central field of view. Reading from Fig. 2(d), at optimum laser power 1.490 mW, the signal-to-noise ratio goes to one at microwave power of -47 dBm at microwave generator. As the switch and the microwave wires measured to be -6 dB in transmission (Fig. S5(a)), the microwave power at one port of the microwave transmission line is thus -53 dBm. Though the transmission (reflection) of the microwave line is measured about -5.5 dB (-9 dB), as shown in Fig. S5(b), we use the power of -53 dBm at the diamond sample as a conservative estimate, since the positions of losses on the transmission line is not investigated. The current on the transmission line is estimated by

$$I = \sqrt{\frac{2\,P}{R}} \simeq 1.41 \times 10^{-5}\ \mathrm{A}$$

,where P is the power, and $R \approx 50\ \Omega$ is the impedance of the microwave circuit. The fluorescence of NV centers is measured at the position about $r = 20$ μm from the center of transmission line, so the minimum detectable amplitude of the magnetic field is approximately given by

$$B_{\min} = \frac{\mu I}{2\pi r} \simeq 141.6\ \mathrm{nT}$$

where μ is the vacuum permeability. The fluorescence contrast is calculated by the relative difference of detecting and reference EM-CCD frames with exposure time of $t_d = 50$ ms, thus the sensitivity of magnetic field amplitude is approximately given by

$$\eta_{\mathrm{amp}} = B_{\min} \cdot \sqrt{2t_d} \simeq 45\ \mathrm{nT}/\sqrt{\mathrm{Hz}}$$

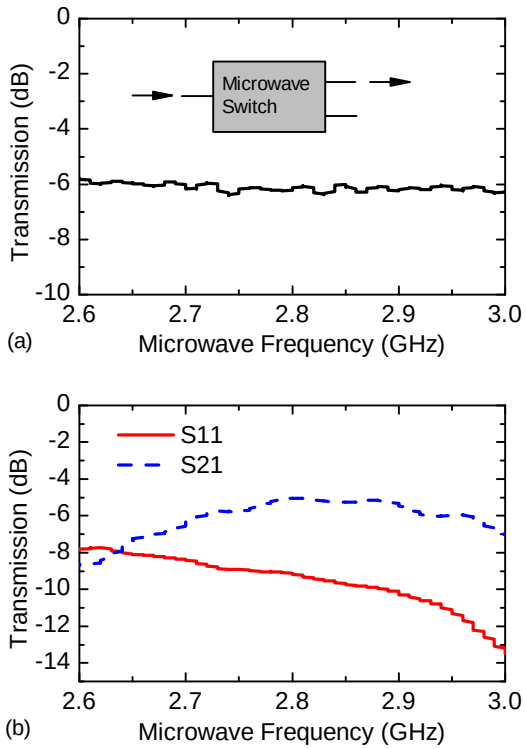

FIG. S5: (a) The transmission of the microwave switch and wires measured by a network analyzer. (b) Reflection (S11) and transmission (S21) of the microwave transmission line on the micro-fabricated circuit used for sensitivity estimation. The ports for measurements are both of 50Ω impedance.

Note 2. THEORETICAL MODEL

As depicted in Fig. S6, the ground and excited states of NV are spin-triplet. For the ground states, there is a zero-field splitting $D_0 = 2.87$ GHz between $|0\rangle_g$ and $|\pm 1\rangle_g$ energy levels. In the presence of a bias magnetic field B, the degeneracy of the $|\pm 1\rangle_g$ energy levels is lifted with the Zeeman shift $\Delta = 2g\mu_B B/h$, where $g\mu_B/h = 28$ MHz/mT is the NV gyromagnetic ratio. Here the magnetic field is aligned with major axis of NV center.

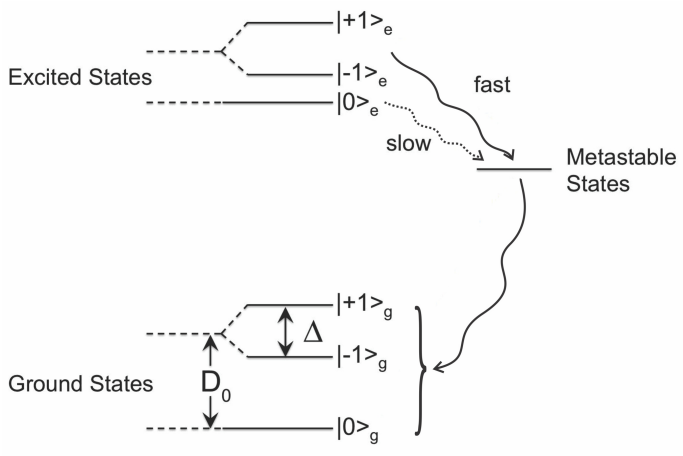

FIG. S6: Energy level diagram of NV centers.

For clarification, we first consider the two-level system, only consisting of the ground states $|0\rangle_g$ and $|1\rangle_g$. The Liouville equation gives the motion for density operator ρ as

$$\dot{\rho} = -\frac{i}{\hbar}[\mathcal{H}, \rho] \tag{S1}$$

When a microwave field is appied, the Hamiltonian of the two-level system is given by [S1]

$$\mathcal{H} = \hbar\omega_0 |0\rangle_{gg}\langle 0| + \hbar\omega_1 |1\rangle_{gg}\langle 1| - (\zeta_{01}|0\rangle_{gg}\langle 1| + \zeta_{10}|1\rangle_{gg}\langle 0|)B_{\rm mw}(t), \tag{S2}$$

where $\zeta_{01} = \zeta_{10}^*$ denotes the matrix element of the NV magnetic dipole moment and $B_{\rm mw}(t)$ is the the microwave magnetic field perpendicular to NV axis. For the amplitude of $B_{\rm mw}$ and the frequency of ν, the microwave magnetic field strength satisfies $B_{\rm mw}(t) = B_{\rm mw}(e^{i\nu t} + e^{-i\nu t})/2$.

Then, the motion of the density matrix elements can be derived as

$$\dot{\rho_{00}} = \frac{i}{\hbar}[\zeta_{01} B_{\rm mw}\rho_{10} - \text{c.c.}], \tag{S3}$$

$$\dot{\rho_{11}} = -\frac{i}{\hbar}[\zeta_{01} B_{\rm mw}\rho_{10} - \text{c.c.}], \tag{S4}$$

$$\dot{\rho_{01}} = -i(\omega_1 - \omega_0)\rho_{01} - \frac{i}{\hbar}\zeta_{01}B_{\mathrm{mw}}[\rho_{00} - \rho_{11}]. \tag{S5}$$

When a laser excitation field is applied, the NV spins are pumped from the ground states into the excited states. In additional to spin-conserving optical transitions between the excited and ground states, there exists a non-radiative decay path through metastable states [S2]. As indicated by Fig. S6, the non-radiative transition rate from excited $|\pm 1\rangle_e$ states to metastable states is much greater than the transition rate from excited $|0\rangle_e$ states to metastable states, resulting in the spin population transfer from the $|\pm 1\rangle_g$ states to the $|0\rangle_g$ states, characterized by the optical polarization rate G_{op} [S3, S4]. With the excitation laser power of P, the optical polarization rate is approximated to be

$$G_{\mathrm{op}} = G_{\mathrm{op,sat}}\frac{P}{P + P_{\mathrm{sat}}}, \tag{S6}$$

where $G_{\mathrm{op,sat}}$ and P_{sat} denote the optical polarization and laser power at saturation, respectively. It is shown that the optical polarization rate is proportional to the laser power for weak laser excitation, i.e., when $P \ll P_{\mathrm{sat}}$.

The NV spins also encounter decoherence in ambient environment. The interactions with other spin impurities, such as the non-zero nuclear spins of the ^{13}C isotope and other nitrogen impurities, lead to the dephasing of the NV spins, represented by the spin dephasing rate γ_2. In our experiment, the linewidth of electron spin resonance is $\Gamma_\nu \approx 500$ kHz for weak microwave and laser excitation. The spin dephasing time is calculated to be $T_2^* = 1/(\pi\Gamma_\nu) \approx 0.6$ μs. In the meantime, spin-lattice relaxation occurs due to the perturbations with lattice phonons, which is characterized by the spin relaxation rate $\gamma_1 = 1/T_1$. The spin relaxation time T_1 of our diamond sample is approximated to be 1 ms. Eq. (S3)-(S5) are then modified to be

$$\dot{\rho_{00}} = -\gamma_1(\rho_{00} - \rho_{11}) + G_{\mathrm{op}}\rho_{11} + \frac{i}{\hbar}[\zeta_{01}B_{\mathrm{mw}}\rho_{10} - \mathrm{c.c.}], \tag{S7}$$

$$\dot{\rho_{11}} = -\gamma_1(\rho_{11} - \rho_{00}) - G_{\mathrm{op}}\rho_{11} - \frac{i}{\hbar}[\zeta_{01}B_{\mathrm{mw}}\rho_{10} - \mathrm{c.c.}], \tag{S8}$$

$$\dot{\rho_{01}} = -i(\omega_1 - \omega_0 - \omega)\rho_{01} - \frac{i}{\hbar}\zeta_{01}B_{\mathrm{mw}}[\rho_{00} - \rho_{11}] - \gamma_2\rho_{01}. \tag{S9}$$

In steady state, the normalized fluorescence at microwave frequency $\nu = \omega/(2\pi)$ satisfies

$$I(\nu) = \rho_{00} + \beta\rho_{11}. \tag{S10}$$

Here β is a factor which indicates the different fluorescence of the two states (i.e., $|0\rangle_g$ and $|1\rangle_g$), and we approximate it to be 0.6.

By sweeping the magnetic field strength, we obtain the dependence of fluorescence on magnetic field. Taking the transition between $|0\rangle_g$ and $|-1\rangle_g$ into account, we obtain the normalized fluorescence as

$$I(B) = 1 - C_0 \sum_{m=\pm1} \frac{(\Gamma/2)^2}{[B + \frac{mh}{g\mu_B}(\nu - D_0)]^2 + (\Gamma/2)^2}, \tag{S11}$$

where the contrast C_0 and the linewidth Γ of the electron spin resonance (ESR) spectra are then given by

$$C_0 = \frac{(1-\beta)\xi_1 G_{\rm op}}{(1+\beta)\gamma_1 + G_{\rm op}} \cdot \frac{2\zeta_{01}^2}{4\zeta_{01}^2 + \gamma_2(2\gamma_1 + G_{\rm op})/(\hbar^2 B_{\rm mw}^2)}, \tag{S12}$$

$$\Gamma = \frac{h}{\pi g \mu_B} \sqrt{\gamma_2(\gamma_2 + \frac{4\zeta_{01}^2 B_{\rm mw}^2}{2\hbar^2(2\gamma_1 + G_{\rm op})})}. \tag{S13}$$

Here we include the resonant ratio $\xi_1 \approx 25\%$ to account for the effects of four possible NV directions.

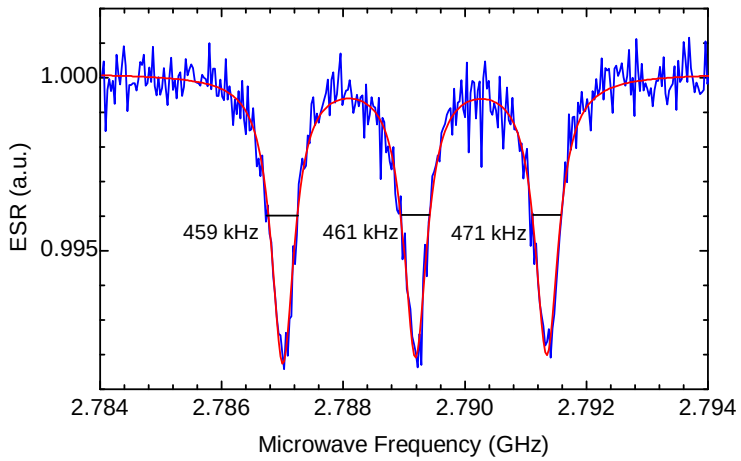

FIG. S7: Electron Spin Resonance of the diamond sample. The linewidth of the individual curve is obtained by fitting to the Lorentz curve. The power of the microwave signal is -20 dBm, and the exposure time of EM-CCD is 30.5 ms.

Generally, the NV spins are in hyperfine interaction with ^{14}N or ^{15}N. Taking ^{15}N for instance, each of the two Lorentzian dips in Eq. (S11) splits into three dips, equally separated by $A_\parallel = 2.16$ MHz. The normalized fluorenscence can then be approximated as

$$I(B) = 1 - \sum_{m=\pm1} \sum_{i=0,\pm1} \frac{C(\Gamma/2)^2}{[B + \frac{mh}{g\mu_B}(\nu - D_0 + iA_\parallel)]^2 + (\Gamma/2)^2}, \tag{S14}$$

where the contrast of a single dip is $C = C_0/3$.

In our experimental configuration, the linewidth of electron spin resonance is $\Gamma_\nu \approx 460$ kHz for weak microwave and laser excitation, as shown in Fig. S7. The spin dephasing time is calculated to be $T_2^* = 1/(\pi\Gamma_\nu) \approx 0.69\,\mu$s. Throughout the supplementary information, we approximate $T_1 = 1$ ms, $G_{\rm sat} = 5\times10^6$ s^{-1}, $P_{\rm sat} = 1.6$ W, $\beta = 0.6$, $\xi_1 = 25\%$ (due to the four NV orientations), and $\xi = \xi_1/3$ (due to hyperfine interaction with ^{15}N) as in the references [S3–S6].

Note 3. MICROWAVE DETECTION

A. Microwave Frequency

By sweeping the magnetic field strength, the spectra of fluorescence is obtained. When the microwave field is on resonance with the transitions between $|0\rangle_g$ and $|\pm1\rangle_g$, dips appear in the spectra. As indicated by Eq. (S11), the unknown microwave field frequency can be derived from the center magnetic field B_0 as

$$\nu = D_0 \pm \frac{g\mu_B}{h}B_0. \tag{S15}$$

When the magnetic field B_0 is fixed, we set the detecting frequency at the position of maximum slope. Then, the small frequency deviation can be retrieved from the fluorescence change. The dynamic range of frequency with mixed magnetic field is given by Δ_ν, related to the ESR linewidth,

$$\Delta_\nu = \frac{g\mu_B}{\sqrt{3}h}\Gamma. \tag{S16}$$

The absolute value of microwave frequency ν is retrieved from the signal, *i.e.*, normalized fluorescence I. The response of fluorescence change to the frequency change, *i.e.* sensitivity, is characterized by the partial derivative of the fluorescence with respect to the microwave frequency, derived as

$$\frac{\partial I}{\partial \nu} = \frac{h}{g\mu_B}\cdot\frac{\partial I(B=\frac{h\nu}{g\mu_B})}{\partial B} = \frac{3C\Delta_\nu^2(\nu+\Delta_\nu/2)}{2[\Delta_\nu^2/4+(\nu+\Delta_\nu/2)^2]^2}. \tag{S17}$$

Fig. S8 depicts how fluorescence changes in response to the microwave frequency derivation. The maximum derivative is calculated from Eq. (S17) as

$$\left|\frac{\partial I}{\partial \nu}\right|_{\rm max} = \frac{3\sqrt{3}hC}{4g\mu_B\Gamma}. \tag{S18}$$

For instance, with the contrast of 1% and the linewidth of 1 MHz, the frequency scope is $\Delta_\nu = 580$ kHz and the maximum derivative is $|\partial I/\partial\nu|_{\rm max} = 0.005\%$ kHz^{-1}.

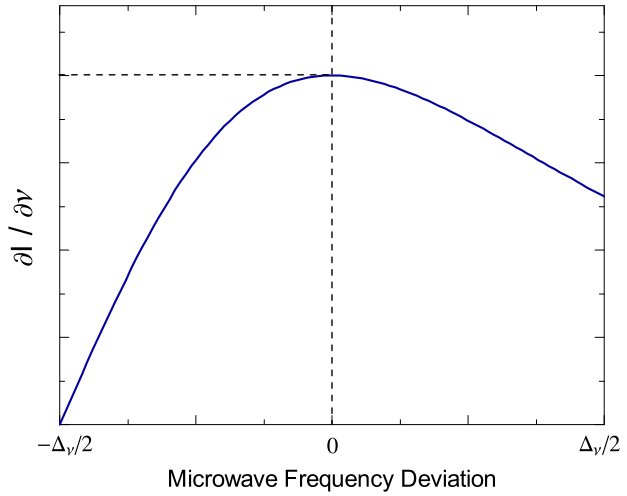

FIG. S8: The partial derivative of fluorescence with respect to frequency derivation $\partial I/\partial\nu$ as a function of frequency deviation.

B. Microwave Power

The microwave power is retrieved from the fluorescence contrast of the spectra. Eq. (S12) can be rewritten in terms of the Rabi frequency $\Omega_R = \zeta_{01} B_{\mathrm{mw}}/\hbar$ as

$$C = \frac{a_0}{1 + a_1/\Omega_R^2}, \tag{S19}$$

where a_0 and a_1 are constants decided by the laser power and NV property.

For weak excitation laser, i.e., $P \ll P_{\mathrm{sat}}$, no significant broadening is induced and the laser power has minor impact on the spin dephasing rate, i.e., $\gamma_2 \approx 1/T_2^*$. In this case, the constants a_0 and a_1 are given by

$$a_0 = \frac{(1-\beta)\xi_1 G_{\mathrm{op}} T_1}{(1+\beta) + G_{\mathrm{op}} T_1}, \tag{S20a}$$

$$a_1 = \frac{(2 + G_{\mathrm{op}} T_1)}{4 T_1 T_2^*}. \tag{S20b}$$

As shown in Fig. S9(a), the fluorescence contrast depends on both the optical polarization rate and the square of the Rabi frequency, i.e., on both the laser power and microwave power. The dependence of contrast on the square of Rabi frequency, which is proportional to the microwave power, and that on the Rabi frequency, which is proportional to the magnetic field amplitude, are depicted in Fig. S9(b), which matches well with our experiment data. The contrast grows monotonically with the increase of the Rabi frequency and a saturation effect is observed when the

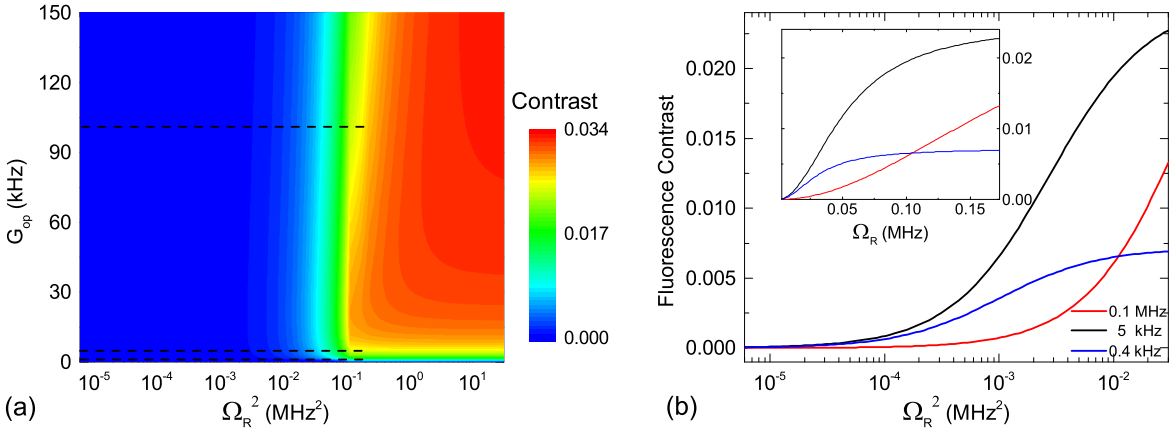

FIG. S9: (a) Theoretical contour plot of fluorescence contrast as a function of optical polarization rate and square of Rabi frequency. (b) Fluorescence contrast vs. square of Rabi frequency for optical polarization rate of 0.1 MHz (red curves), 5 kHz (black curves), and 0.4 kHz (blue curves). The three curves correspond to the dashed curves indicated in (a). Inset: Contrast as a function of the Rabi frequency.

microwave field is strong enough. More specifically, the contrast approaches the value of a_0 when the Rabi frequency exceeds far more than the value of a_1, as indicated by Eq. (S12).

Similar to the discussion of microwave frequency detection above, the sensitivity of detecting microwave power, described by Ω_R^2, is given by

$$\frac{\partial C}{\partial \Omega_R^2} = \frac{a_0}{a_1(1+\Omega_R^2/a_1)^2}. \tag{S21}$$

Eq. (S21) indicates a monotonic decrease of the derivative with the growth of the microwave power. However, in some applications, *e.g.* spectrum analysis, we prefer a logarithmic unit of microwave power, such as dBm. In this case, the sensitivity of microwave power detection is given by,

$$\frac{\partial C}{\partial \log\left(\Omega_R^2\right)} = \frac{a_0\Omega_R^2}{a_1(1+\Omega_R^2/a_1)^2}. \tag{S22}$$

The derivative $\partial C/\partial \log\left(\Omega_R^2\right)$ has a non-monotonic dependence on the square of the Rabi frequency as depicted in Fig. S10. The constants a_0 and a_1, given by Eq. (S20), are the characteristic values of the fluorescence contrast and the square of the Rabi frequency, respectively.

Note 4. MICROWAVE FREQUENCY SENSITIVITY

The measurement precision is limited by noises, which are mainly from pump laser fluctuations and electronic devices in our experiment. For a measurement with N photons collected, the photon

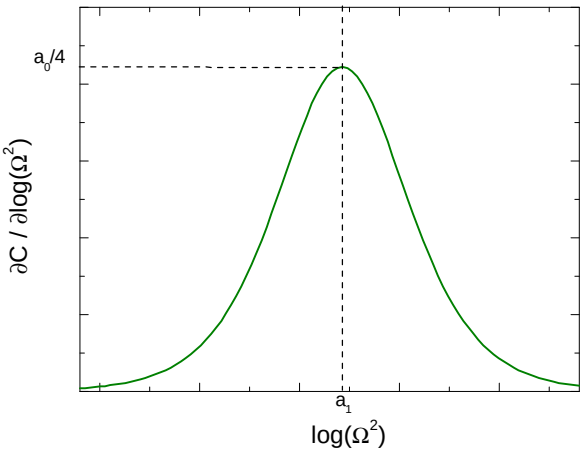

FIG. S10: The sensitivity in microwave power detection on the squared Rabi frequency in logarithmic unit.

noise is set to be δN. In microwave frequency detection, the normalized fluorescence is utilized as our signal. The minimum detectable frequency change is then given by

$$\delta\nu = \frac{1}{\left|\frac{\partial I}{\partial \nu}\right|} \cdot \frac{\delta N}{N}, \tag{S23}$$

The sensitivity of microwave frequency is then determined by

$$\eta_\nu = \delta\nu\sqrt{t_m} = \frac{1}{\left|\frac{\partial I}{\partial \nu}\right|} \cdot \frac{\delta N\sqrt{t_m}}{N}, \tag{S24}$$

where t_m is the measurement time. Note that the photon collection rate, defined as the number of photons collected per second, is given by $n = N/t_m$. In Eq. (S24), the term $\delta N\sqrt{t_m}/N$ varies for different experiment setup and for different kinds of noise sources. Taking the shot noise for example, we consider it to be the dominant noise sources, with $\delta N \approx \sqrt{N}$. Here we assume the detecting frequency is at the position of maximum slope. To analyze the influence of the microwave power on the detection sensitivity, we first express the linewidth Γ in terms of the Rabi frequency as

$$\Gamma = \frac{h\gamma_2\sqrt{1+\Omega_R^2/a_1}}{\pi g\mu_B}. \tag{S25}$$

For the weak excitation, the microwave frequency sensitivity is calculated as

$$\eta_\nu = \frac{4}{3\sqrt{3}\pi a_0 T_2^*\sqrt{n}} \cdot \frac{(1+\Omega_R^2/a_1)^{3/2}}{\Omega_R^2/a_1}. \tag{S26}$$

As shown in Fig. S11, the detection sensitivity of microwave frequency depends heavily on the microwave field strength. When the Rabi frequency, i.e., the microwave power, is increased, the

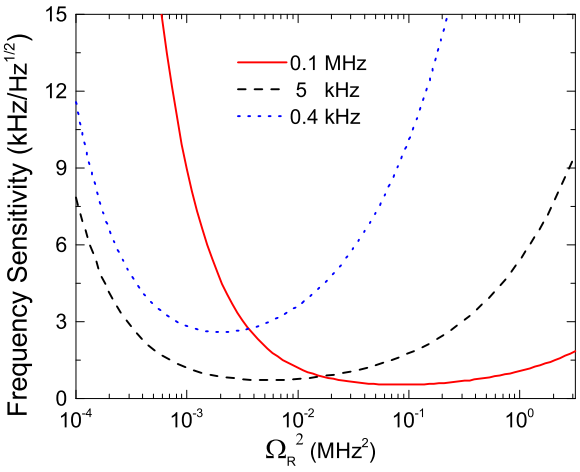

FIG. S11: Frequency sensitivity vs. microwave power for optical polarization rate of 0.1 MHz (red solid curve), 5 kHz (black dashed curve), and 0.4 kHz (blue dotted curve). The photon collection rate n is approximate to be 10^5.

resonance contrast C grows while the linewidth Γ is broadened. It is also known from Eqs. (S18) and (S26) that the sensitivity is proportional to Γ/C. Thus, the trade-off between the increased contrast and the broadened linewidth leads to an optimal Rabi frequency value for the smallest sensitivity. Similarly, strong laser excitation also leads to large contrast and broad linewidth, which results in a trade-off effect of laser strength on detection sensitivity. Besides, Fig. S11 illustrates that the microwave frequency detection sensitivity can be lower than 1 kHz/$\sqrt{\text{Hz}}$ using the experimental parameters extracted from our measurements.

[S1] L. Mandel and E. Wolf, *Optical coherence and quantum optics* (Cambridge university press, 1995).

[S2] N. B. Manson, J. P. Harrison, and M. J. Sellars, Physical Review B **74**, 104303 (2006).

[S3] L. Robledo, H. Bernien, T. van der Sar, and R. Hanson, New Journal of Physics **13**, 025013 (2011).

[S4] A. Dréau, M. Lesik, L. Rondin, P. Spinicelli, O. Arcizet, J.-F. Roch, and V. Jacques, Phys. Rev. B **84**, 195204 (2011).

[S5] V. M. Acosta, E. Bauch, M. P. Ledbetter, C. Santori, K.-M. C. Fu, P. E. Barclay, R. G. Beausoleil, H. Linget, J. F. Roch, F. Treussart, et al., Phys. Rev. B **80**, 115202 (2009).

[S6] M. L. Goldman, A. Sipahigil, M. W. Doherty, N. Y. Yao, S. D. Bennett, M. Markham, D. J. Twitchen, N. B. Manson, A. Kubanek, and M. D. Lukin, Phys. Rev. Lett. **114**, 145502 (2015).